Quantum criticality of reconstructing Fermi surfaces

Junhyun Lee, Philipp Strack,* and Subir Sachdev

Department of Physics, Harvard University, Cambridge MA 02138

(Dated: September 24, 2012)

We present a functional renormalization group analysis of a quantum critical point in a two-dimensional metal involving Fermi surface reconstruction due to the onset of spin density wave order. The critical theory is controlled by a fixed point in which the order parameter and fermionic quasiparticles are strongly coupled, and acquire spectral functions with a common dynamic critical exponent. We obtain results for critical exponents, and for the variation in the quasiparticle spectral weight around the Fermi surface.

Introduction. Quantum phase transitions between two Fermi liquids, one of which spontaneously breaks translational symmetry and so reconstructs its Fermi surface, have been of long standing theoretical and experimental interest. Important new examples of experimental realizations have emerged in the past few years [1–3], and so a full theoretical understanding is of some urgency. However, despite several decades of theoretical work, key questions remain open especially in the important case of two spatial dimensions.

Early theories [4–9] for such quantum phase transitions focused on effective models for the quantum fluctuations of the order parameter, while treating the Fermi surface reconstruction as an ancillary phenomenon. However, it has since become clear [10] that such an approach is inadequate, and the Fermi surface excitations are primary actors in the critical theory. Ref. 11 postulated a critical theory for Fermi surface reconstruction, in which the Fermi surface excitations and the bosonic order parameter were equally important and both acquired anomalous dimensions. These excitations were strongly coupled to each other by a 'Yukawa' coupling of universal strength, and their correlators scaled with a common dynamic critical exponent, z. Explicit computations were performed in the context of a $1/N$ expansion (where N is the number of fermion flavors) for the onset of spin density wave order, but no such critical theory appeared at the two-loop level. Indeed, it was pointed out that at higher loops [11–13] there is a breakdown of the $1/N$ expansion, and so it remained unclear whether the postulated fixed point existed.

Here we will address the problem of Fermi surface reconstruction at the onset of spin density wave order by an analysis based on a formally exact functional renormalization group approach [14, 15]. In an approximation where we truncate the flow equations to a set of discrete points on the Fermi surface and keep the shape of the Fermi surface fixed, we establish the existence of a fixed point with the scaling structure postulated in Ref. 11, describing the quantum phase transition between two Fermi liquids. A significant feature of this method is that it ties the parameters controlling the order parameter fluctuations to those associated with the fermion excitations, and this is important for a proper description of the scaling structure. We present numerical results for the critical exponents of the boson and fermion spectral functions, and for the variation in the fermionic quasiparticle residue around the Fermi surface.

Model. Our computation will be carried in the context of the 'spin-fermion' model of antiferromagnetic fluctuations in a Fermi liquid [9]. This involves a spin density wave order parameter $\vec{\phi}$ at wavevector $\mathbf{K} = (\pi, \pi)$ coupled to fermions Ψ moving on a square lattice. The analytic analyses have focused on the vicinity of the 'hot spots' on the Fermi surface: these are the 8 points on the Fermi surface which can generically be connected to each other by $\mathbf{K}$. The fermion dispersions were linearized and truncated around the hot spots. However a complete analysis requires that we avoid the spurious singularities associated with truncated Fermi surfaces, and deal only with continuous Fermi surfaces. Here, we will choose the Fermi surface configurations of a recent analysis [16] which allowed Monte Carlo studies without a sign problem. This paves the way for an eventual comparison of our renormalization group results with Monte Carlo. Our present method applies also to general Fermi surfaces, and provides access to real-time spectral functions which are not easily obtainable from imaginary-time Monte Carlo.

The model of Ref. [16] contains fermions in two bands, Ψ_α, $\alpha = 1, 2$ (although our present method can also be applied to single band models) coupled to $\vec{\phi}$ in the effective action

$$
\Gamma^{\Lambda_{\mathrm{UV}}}\left[\bar{\psi}, \psi, \vec{\phi}\right] = \int_k \sum_{\alpha=1,2} \overline{\Psi}_\alpha(k) \begin{pmatrix} -ik_0 + \xi_{\mathbf{k},\alpha} & 0 \\ 0 & -ik_0 + \xi_{\mathbf{k},\alpha} \end{pmatrix} \Psi_\alpha(k)
$$
$$
+ \int_q \frac{1}{2} \vec{\phi}(-q) \left(\mathbf{q}^2 + r\right) \vec{\phi}(q) \tag{1}
$$
$$
+ \int_{k,q} \lambda \vec{\phi}(q) \left(\overline{\Psi}_1(k+q)\vec{\sigma}\,\Psi_2(k) + \overline{\Psi}_2(k+q)\vec{\sigma}\Psi_1(k)\right)
$$

where $\int_k$ represents integrals over spatial momenta $\mathbf{k} = (k_x, k_y)$ over the Brillouin zone, and over frequencies k_0. The fermion spinors are defined by $\overline{\Psi}_\alpha(k) = (\bar{\psi}_{\alpha,\uparrow}(k)\ \bar{\psi}_{\alpha,\downarrow}(k))$, $\alpha = 1, 2$. We already introduce here the cutoff Λ along which we later integrate our renormalization group flow toward $\Lambda \to 0$. With $\Lambda = \Lambda_{\mathrm{UV}}$ we have the bare lattice action. The boson quadratic terms consists of the control parameter r and a spatial gradient squared to account for spatial variations of the order parameter field $\vec{\phi}$. The quantum dynamics of $\vec{\phi}$ will be generated in the RG flow; putting a q_0^2 term into Eq. (1) does not change our results. The fermion dispersions for nearest-neighbor hopping
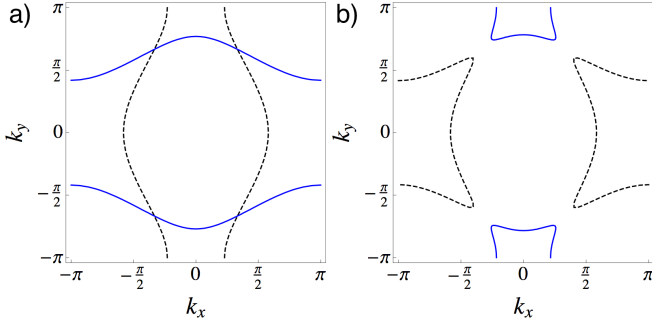
FIG. 1: (Color online) Reconstructing Fermi surfaces ($\xi_{\mathbf{k},1} = 0$, black-dashed line; $\xi_{\mathbf{k},2} = 0$, blue-solid line for Eq. (2)) from the paramagnetic phase (a) to the zeros of the quasi-particle energies in the antiferromagnetic (SDW) phase (b). Gaps open at the 'hot spots', that is, where the Fermi surfaces of the two flavors intersect. In this paper, we focus on the SDW transition that is the singular point right when the Fermi surfaces reconstruct. The C_4 lattice symmetry of the original fermions is preserved.

are

$$\xi_{\mathbf{k},\alpha} = -2t_{\alpha,x}\cos k_x - 2t_{\alpha,y}\cos k_y - \mu_\alpha. \quad (2)$$

A consistent mapping to "physical" fermions can be achieved with the an anisotropic choice of hoppings [16], $t_> = 1$ and $t_< = 0.5$ and: $t_{1,x} = t_>$, $t_{2,x} = -t_<$, $t_{1,y} = t_<$, $t_{2,y} = -t_>$ yielding the Fermi surfaces shown in Fig. 1.

A mean-field analysis of Eq. (1) predicts an antiferromagnetic spin-density wave (SDW) ground state at $r = 1.34$ which spontaneously breaks the spin SU(2) symmetry of Eq. (1). The Fermi surface topology "reconstructs" and gaps open at the hot spots as shown in Fig. 1. On a mean-field level, the SDW transition at zero temperature of Eq. (1) is first order, as was also found in related single-band models for electronic antiferromagnets [17, 18]. In the present paper, we however focus on continuous SDW transitions at zero temperature.

Key results. We now describe the three key results of this paper. (i) We find an infrared strong-coupling fixed point for the Yukawa-coupling λ^Λ which governs the RG flow of the coupled Fermi-Bose action down to the lowest scales $\Lambda \to 0$. This induces scaling relations among the anomalous exponents for the Fermi velocity, the quasi-particle weight and the Yukawa vertex. (ii) Both the quasi-particle weight and the Fermi velocity vanish as a power-law when scaling the momenta toward the hot spot; the Fermi velocity slower than the quasi-particle weight. (iii) The (quantum) dynamical scaling of the electronic single-particle and collective spin fluctuations follows from an emergent dynamical exponent attaining the same (fractional) value for both, fermions and boson.

As explained in more detail in the Supplemental Material, our RG analysis is based on the (formally exact) flow equation for the effective action $\Gamma_R^\Lambda[\bar{\psi}, \psi, \vec{\phi}]$, the generating functional for one-particle irreducible correlation functions in the form derived by Wetterich [14, 15]. The regulator R introduces a cutoff dependence into the effective action so that Γ_R^Λ

smoothly interpolates between the bare action, Eq. (1), at the ultraviolet scale $\Gamma_R^{\Lambda=\Lambda_{UV}}[\bar{\psi}, \psi, \vec{\phi}] = \Gamma^{\Lambda_{UV}}[\bar{\psi}, \psi, \vec{\phi}]$ and the fully renormalized effective action in the limit of vanishing cutoff: $\lim_{\Lambda\to 0} \Gamma_R^\Lambda[\bar{\psi}, \psi, \vec{\phi}] = \Gamma[\bar{\psi}, \psi, \vec{\phi}]$. The Wetterich equation has a one-loop structure and in a vertex expansion the β-functions for the n-point correlators are determined by (cutoff derivatives of) one-particle irreducible one-loop diagrams with fully dressed propagators and vertices. Upon self-consistent integration of the coupled set of β-functions, contributions of arbitrary high loop order are generated. In this paper, we truncate the effective action to the full fermion two-point function (including a fermion self-energy $\Sigma_f^\Lambda(k_0, \mathbf{k})$), the full bosonic two-point function (including a bosonic self-energy $\Sigma_b^\Lambda(q_0, \mathbf{q})$), and the Yukawa coupling λ^Λ.

The centerpiece of our analysis is the flow equation for the Yukawa coupling:

$$\Lambda\partial_\Lambda\tilde{\lambda}^\Lambda = \left(\frac{1}{4}\left(\eta_{Z_{f1}} + \eta_{Z_{f2}} + \eta_{A_{f1}} + \eta_{A_{f2}}\right) - \eta_{\text{yuk}} - \frac{1}{2}\right)\tilde{\lambda}^\Lambda , \quad (3)$$

where $\left(\tilde{\lambda}^\Lambda\right)^2 = \left(\lambda^\Lambda\right)^2/(\Lambda\sqrt{Z_{f1}^\Lambda Z_{f2}^\Lambda}\sqrt{A_{f1}^\Lambda A_{f2}^\Lambda})$ is rescaled by the frequency (Z_{f1}^Λ) and momentum (A_{f1}^Λ) derivatives of the fermion self-energy generated under the RG flow as per Fig. 2 (a). The power-law divergences as well as all other non-universal contributions to the flow of the two fermion self-energy factors and the Yukawa coupling itself are absorbed into the anomalous exponents:

$$\eta_{Z_{f1}} = -\frac{d\log Z_{f1}^\Lambda}{d\log\Lambda} , \quad \eta_{A_{f1}} = -\frac{d\log A_{f1}^\Lambda}{d\log\Lambda} , \quad \eta_{\text{yuk}} = -\frac{d\log\lambda^\Lambda}{d\log\Lambda} . \quad (4)$$

η_{yuk} is driven by the direct contribution to the flow of λ^Λ exhibited in Fig. 2 (b). All couplings are projected to zero fermionic frequency, a discrete set of fermionic momenta on the Fermi surfaces, and zero bosonic frequency and momenta. This is where the most singular renormalizations occur.
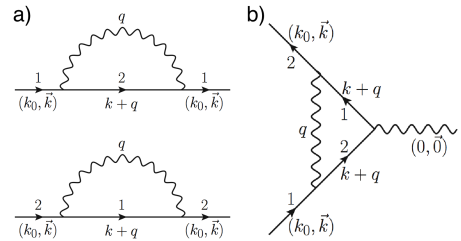

FIG. 2: Diagrammatic representation of the flow equation for the fermion self-energy $\Sigma_f^\Lambda(k_0, \mathbf{k})$ (a) and the Yukawa coupling (b). Straight lines denote Fermi propagators of flavor 1 and 2, wiggly lines boson propagators are endowed with a regulator R^Λ (specified in the Supplemental Material). Intersections of wiggly with straight lines represent the Yukawa coupling. The cutoff-derivative with respect to R^Λ is implicit. All propagators and vertices are "dressed" self-consistently and are functions of Λ.

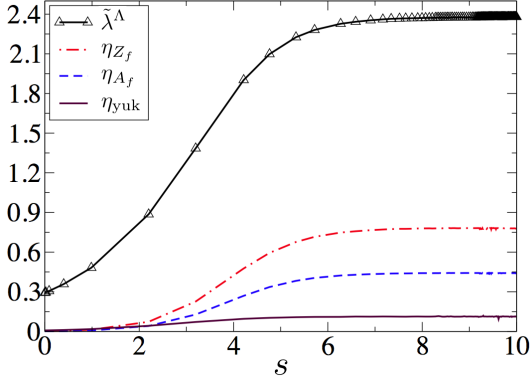FIG. 3: (Color online) Quantum critical RG flows of the Yukawa coupling and the anomalous exponents at the hot spot $\mathbf{k}_{\mathrm{HS}}$. The fixed-point values are $\tilde{\lambda}^\Lambda = 2.38$, $\eta_{Z_f} = 0.78$, $\eta_{A_f} = 0.44$ and $\eta_{\mathrm{yuk}} = 0.11$. The scaling plateaus for $s \gtrsim 6$ depicted over ~ 4 orders of magnitude would be attained indefinitely but are limited by the numerics only. The infrared is to the right of the plot ($\Lambda = \Lambda_{\mathrm{UV}} e^{-s}$).

Specifically, the inverse quasi-particle weight is computed from the flowing self-energy by [19]

$$Z_{f1}^\Lambda = 1 - \frac{\partial}{\partial i k_0} \Sigma_{f1}^\Lambda(k_0, \mathbf{k})|_{k_0=0, \mathbf{k}=\mathbf{k}_{\mathrm{F}}} \qquad (5)$$

where $\mathbf{k}_{\mathrm{F}}$ is a momentum on the Fermi surface and the initial condition is $Z_{f1}^{\Lambda_{\mathrm{UV}}} = 1$. The momentum renormalization factor is obtained from a momentum gradient of the fermion self-energy

$$A_{f1}^\Lambda = 1 + \frac{|\mathbf{n}_{\mathbf{k},1} \cdot \nabla \Sigma_{f1}^\Lambda(k_0, \mathbf{k})|}{|\nabla \xi_{\mathbf{k},1}|}\Bigg|_{k_0=0, \mathbf{k}=\mathbf{k}_{\mathrm{F}}}, \qquad (6)$$

with the initial condition $A_{f1}^{\Lambda_{\mathrm{UV}}} = 1$. Here, $\nabla = (\partial_{k_x}, \partial_{k_y})$ and $\mathbf{n}_{\mathbf{k},1}$ is unit normal vector onto the Fermi surface of flavor 1. We shall see below that the momentum gradient scales differently than the frequency derivative at the quantum critical point. In a different context, for Fermi systems with van Hove singularities, this asymmetry was established to all orders in perturbation theory by Feldman and Salmhofer [20]. Necessary conditions to discover this are: (i) the co-dimension of the Fermi surface manifold is greater than zero (it is zero in a one-dimensional Fermi systems) and (ii) one includes the additional, relevant transversal momentum direction parallel to the Fermi surface into the analysis.

With these definitions, the scale-dependent "dressed" fermion propagator which occurs self-consistently in all RG equations becomes

$$G_{f1}^\Lambda(k) = \frac{-1}{-ik_0 + \xi_{\mathbf{k},1} + \Sigma_{f1}^\Lambda(k_0, \mathbf{k})} = \frac{\mathcal{Z}_{f1}^\Lambda}{ik_0 - |\upsilon_{f1}^\Lambda|\xi_{\mathbf{k},1}}, \qquad (7)$$

with $\mathcal{Z}_{f1}^\Lambda = 1/Z_{f1}^\Lambda$ resembling the quasi-particle weight at low energies and the effective modulus of the Fermi velocity $|\upsilon_{f1}^\Lambda| = \frac{A_{f1}^\Lambda}{Z_{f1}^\Lambda}$.

A self-consistent numerical solution of the flow equations for the Yukawa vertex λ^Λ, the fermion self-energy $\Sigma_f^\Lambda(k_0, \mathbf{k})$ and the boson self-energy $\Sigma_b^\Lambda(q_0, \mathbf{q})$ (to be described below) is attracted toward an infrared strong-coupling fixed point. As can be read off from Fig. 3, the β-function for the Yukawa coupling, Eq. (3), vanishes for $s \gtrsim 6$ resulting in a scaling relation for the fermion and Yukawa anomalous exponents:

$$\frac{d \log \tilde{\lambda}^\Lambda}{d \log \Lambda} = 0 \quad \Leftrightarrow \quad \frac{1}{2}\left(\eta_{Z_f} + \eta_{A_f}\right) = \eta_{\mathrm{yuk}} + \frac{1}{2}, \qquad (8)$$

where we dropped the flavor index as they become degenerate at the hot spot. A similar strong-coupling fixed-point and scaling relations (without singular vertex corrections) have recently been obtained at the QCP of Dirac cone toy model between a semimetal and a superfluid [21].

The numerical values of the exponents (see Fig. 3) determine the scaling behavior of the fermion propagator Eq. (7) and the associated dynamical exponent z_f. The Yukawa vertex diverges as a power-law

$$\lambda^{\Lambda \to 0} \sim \frac{1}{\Lambda^{\eta_{\mathrm{yuk}}}} = \frac{1}{\Lambda^{0.11}}. \qquad (9)$$

Λ can be associated with the momentum distance from the hot spot; at $\Lambda = 0$ the hot spots are resonantly connected by the ordering wave vector $\mathbf{K}$ of the incipient spin-density wave. At the hot spot, the fermionic quasi-particle weight vanishes as a power-law:

$$\mathcal{Z}_f^{\Lambda \to 0} \sim \Lambda^{\eta_{Z_f}} = \Lambda^{0.78} \qquad (10)$$

destroying the Fermi liquid character of fermionic quasi-particle excitations. In a non-selfconsistent calculation we can also compute the fermion self-energy from Eq. (5) away from the hot spot by solving the flow equations evaluated at general
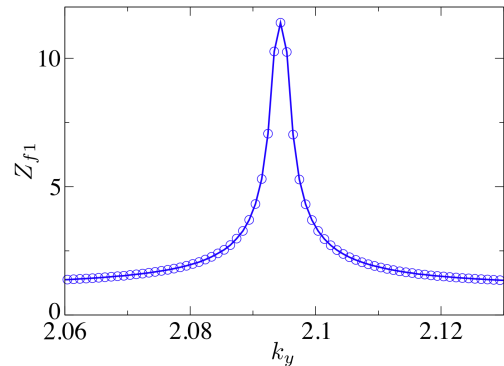

FIG. 4: (Color online). Infrared values of the momentum resolved inverse quasi-particle weights $Z_{f1}^{\Lambda \to 0}[k_0 = 0, k_x, k_y]$ non-selfconsistently computed from Eq. (5) along the Fermi surface. Fig. 5 exhibits flows of the corresponding exponents for the six data points closest to the maximum/hot spot on the right flank. Here the hot spot is located at $k_{\mathrm{HS},y} = 2.0944$ and $k_{\mathrm{HS},x} = 1.0472$.
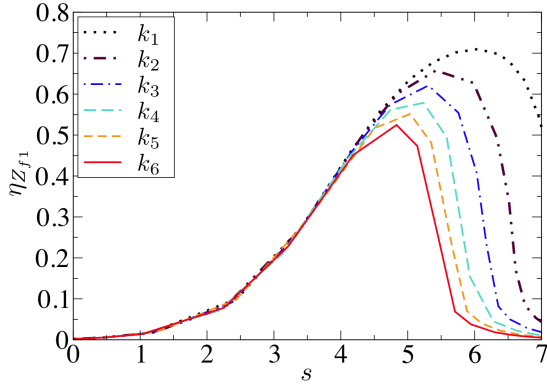
FIG. 5: (Color online). Non-fermi liquid regimes at intermediate scales of the anomalous exponent for the quasi-particle weight $\eta_{Z_{f1}}[k_0 = 0, k_x, k_y]$ for six choices of momenta progressively approaching the hot spot (corresponding to the 6 data points closest to the maximum/hot spot on the right flank of Fig. 4). The momentum $\mathbf{k}_6$ is furthest from the hot spot and $\mathbf{k}_1$ is closest to it. The infrared is to the right of the plot ($\Lambda = \Lambda_{\mathrm{UV}} e^{-s}$).

fermionic momenta $\mathbf{k}$. The result for a momentum cut along the Fermi surface is exhibited in Fig. 4. The renormalization of the quasi-particle weight is strongly peaked around the intersection of the Fermi surfaces at the hotspot. Away from the hot spot, the suppression of the quasi-particle weight is less pronounced leading to asymptotically vanishing anomalous exponents in the infrared $\Lambda \to 0$ (Fig. 5). Nevertheless, in the vicinity of the hot spot, magnetic fluctuations are still very strong leading to sizable non-Fermi liquid scaling regimes at intermediate scales with the maximum progressively approaching the hot spot value $\eta_{Z_{f1}}[k_0 = 0, k_x = k_{\mathrm{HS},x}, k_y = k_{\mathrm{HS},y}] = 0.78$ for momenta closer to it.

In the numerics for Fig. 4, we stopped the flow at $s = 7$ (recall that $\Lambda = \Lambda_{\mathrm{UV}} e^{-s}$) leading to finite (but very large) values of Z_{f1} even at the hot spot. We used a momentum cut of 100 points producing for each grid point in Fig. 4 the scale-resolved flows shown in Fig. 5.

The Fermi velocity vanishes as well but with a smaller exponent

$$|v_f^{\Lambda \to 0}| \sim \Lambda^{\eta_{Z_f} - \eta_{A_f}} = \Lambda^{z_f - 1} = \Lambda^{0.34} , \quad (11)$$

so that the dynamical exponent for the fermions is

$$z_f = 1 + \eta_{Z_f} - \eta_{A_f} = 1.34 . \quad (12)$$

An important ingredient to the scaling laws above is the self-consistently flowing boson propagator

$$D^R(q_0, \mathbf{q}) = \frac{-1}{\mathbf{q}^2 + r + \Sigma_b^{\Lambda}(q_0, \mathbf{q}) + R^{\Lambda}} , \quad (13)$$

where R^{Λ} is an infrared momentum regulator that vanishes for $\Lambda \to 0$. The flow equation for the bosonic self-energy $\Sigma_b^{\Lambda}(q_0, \mathbf{q})$ is a convolution of two fermion propagators with
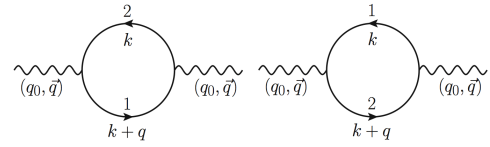

FIG. 6: Particle-hole bubbles used for the flow of the boson self-energy in Eq. (13). All propagators and vertices are "dressed" self-consistently and depend on Λ.

two Yukawa vertices (Fig. 6). The asymptotic static and dynamic scaling of the spin fluctuation propagator is given by

$$\lim_{\Lambda \to 0} \left[D^R(q_0, \mathbf{q}) \right]^{-1} \sim \Lambda^{\eta_{Z_b}} |q_0| + \mathbf{q}^2 \sim |q_0|^{1.66} + \mathbf{q}^2 . \quad (14)$$

with $\eta_{Z_b} = 0.66$. Remarkably, the boson dynamical exponent

$$z_b = 2 - \eta_{Z_b} = 1.34 = z_f , \quad (15)$$

takes the same value as the fermion dynamical exponent. It is a distinguishing feature of this infrared fixed-point of electrons in metals at a spin-density wave transition that the dynamical exponent attains fractional value different from 1 (which is the exact value for quantum-critical fermion systems with Lorentz-symmetry, see Ref. [22] and references therein) and different from 2 (which is the mean-field value of the Hertz theory [5]). Our fermion anomalous dimensions and z can be mapped to those of Ref. 11 for values of the Fermi velocity-anisotropy in a range around $\alpha \approx 0.5$, and upon ignoring the marginal RG flow of α (which is implicitly assumed in (6)); our boson anomalous dimension renormalizing the $\mathbf{q}^2$ term in the propagator is essentially zero, and we trace this to differences in the RG scheme from Ref. 11.

It would be interesting to classify all relevant operators to our fixed point, and investigate the stability of our strong-coupling fixed point further. As a first simple step in this direction, we have extended the truncation for the fermion dispersions to allow for changes in the Fermi surface curvature (keeping the position of the hot spot fixed). A scale-dependent $\tilde{\alpha}^{\Lambda}$ that modifies the hoppings, $t_{1,x/y} \to t_{1,x/y} + \tilde{\alpha}^{\Lambda}$ and $t_{2,x/y} \to t_{2,x/y} - \tilde{\alpha}^{\Lambda}$, does the job. We found only relatively small, finite renormalizations of $\tilde{\alpha}^{\Lambda}$. However, a proper self-consistent investigation of a flowing Fermi surface with the full dispersion used in this paper requires an advanced truncation and likely also a self-consistent determination also of the position of the Fermi surfaces and the hotspots as a function of Λ. Potential tendencies toward magnetic ordering at incommensurate wave vectors might also be captured that way. Such a state-of-the-art truncation was recently presented for self-energy flows in the repulsive Hubbard model close to van Hove filling [23].

Other promising future directions are the inclusion of (d-wave) superconductivity [24], an extension to the quantum-critical regime at finite temperatures, and the exploration of the antiferromagnetic phase with broken symmetry close to the quantum critical point [30].

---

* Electronic address: pstrack@physics.harvard.edu

[1] L. Taillefer, Annual Review of Condensed Matter Physics **1**, 51 (2010); N. Doiron-Leyraud and L. Taillefer, arXiv:1204.0490.

[2] T. Helm *et al.*, Phys. Rev. Lett. **105**, 247002 (2010).

[3] Y. Nakai *et al.*, Phys. Rev. Lett. **105**, 107003 (2010).

[4] A. W. Overhauser Phys. Rev. **128**, 1437 (1962).

[5] J. A. Hertz, Phys. Rev. B **14**, 1165 (1976).

[6] T. Moriya, *Spin Fluctuations in Itinerant Electron Magnetism*, Springer-Verlag, Berlin (1985).

[7] A. J. Millis, Phys. Rev. B, **48**, 7183 (1993).

[8] S. Sachdev, A. V. Chubukov, and A. Sokol, Phys. Rev. B **51**, 14874 (1995).

[9] Ar. Abanov, A. V. Chubukov, J. Schmalian, Adv. Phys. **52**, 119 (2003).

[10] Ar. Abanov and A. V. Chubukov, Phys. Rev. Lett. **84**, 5608 (2000); *Ibid* **93**, 255702 (2004).

[11] M. A. Metlitski and S. Sachdev, Phys. Rev. B **82**, 075128 (2010).

[12] S.-S. Lee, Phys. Rev. B **80**, 165102 (2009).

[13] M. A. Metlitski and S. Sachdev, Phys. Rev. B **82**, 075127 (2010).

[14] W. Metzner *et al.*, Rev. Mod. Phys. **84**, 299 (2012).

[15] J. Berges, N. Tetradis, and C. Wetterich, Physics Reports **363**, 223 (2002).

[16] E. Berg, M. Metlitski, and S. Sachdev, arXiv:1206.0742 (2012).

[17] J. Reiss, D. Rohe, and W. Metzner, Phys. Rev. B **75**, 075110 (2007).

[18] B. L. Altshuler, L. B. Ioffe, and A. J. Millis, Phys. Rev. B **52**, 5563 (1995).

[19] C. Honerkamp and M. Salmhofer, Phys. Rev. B **67**, 174504 (2003).

[20] J. Feldman and M. Salmhofer, Rev. Math. Phys. **20**, 275 (2008).

[21] P. Strack, S. Takei, and W. Metzner, Phys. Rev. B **81**, 125103 (2010); B. Obert, S. Takei, and W. Metzner, Ann. Phys. (Berlin) **523**, 621 (2011).

[22] L. Janssen and H. Gies, arXiv:1208.3327 (2012).

[23] K. U. Giering and M. Salmhofer, arXiv:1208.6131 (2012).

[24] A. Sedeki, D. Bergeron, and C. Bourbonnais, Phys. Rev. B **85**, 165129 (2012).

[25] P. Strack, R. Gersch, and W. Metzner, Phys. Rev. B **78**, 014522 (2008).

[26] F. Schuetz, L. Bartosch, and P. Kopietz, Phys. Rev. B **72**, 035107 (2005).

[27] C. Drukier, L. Bartosch, A. Isidori, and P. Kopietz, Phys. Rev. B **85**, 245120 (2012).

[28] H. Gies and C. Wetterich, Phys. Rev. D **65**, 065001 (2002).

[29] F. Wegner, Grassmann-Variable, Lecture Notes, http://www.tphys.uni-heidelberg.de/~wegner/Vorl09_10.html, Universität Heidelberg (1998).

[30] For example, by generalizing Ref. 25 from the superfluid $O(2)$ case to the staggered $O(3)$ case for the spin-fermion model.

SUPPLEMENTAL MATERIAL

Our results are obtained from the renormalization group flow of the action Eq. (1) at the quantum-critical point ($r = 0$) under the formally exact evolution equation [14]

$$\frac{d}{d\Lambda} \Gamma_R^\Lambda [\chi, \bar{\chi}] = \frac{1}{2} \text{Str} \left\{ \dot{R}^\Lambda \left[\Gamma_R^{(2)\Lambda} [\chi, \bar{\chi}] + R^\Lambda \right]^{-1} \right\} . \quad (16)$$

$\Gamma_R^{(2)\Lambda}$ is the second derivative with respect to the fields defined below. R^Λ is a matrix containing Λ-dependent cutoff functions that regularizes the infrared singularities of the fermion and boson propagators. The dot is short-hand notation for a scale-derivative $\dot{R}^\Lambda = \partial_\Lambda R^\Lambda$. Both sides of this equation are projected onto a "super"-field basis $\chi, \bar{\chi}$ containing fermionic and bosonic entries:

$$\chi(k) = \begin{pmatrix} \phi_x(k) \\ \phi_y(k) \\ \phi_z(k) \\ \psi_{1,\uparrow}(k) \\ \psi_{1,\downarrow}(k) \\ \bar{\psi}_{1,\uparrow}(k) \\ \bar{\psi}_{1,\downarrow}(k) \\ \psi_{2,\uparrow}(k) \\ \psi_{2,\downarrow}(k) \\ \bar{\psi}_{2,\uparrow}(k) \\ \bar{\psi}_{2,\downarrow}(k) \end{pmatrix} \quad (17)$$

and its conjugate-transposed $\bar{\chi}(k)$. Str is a "super" trace over frequency, momenta, and internal indices and installs an additional factor of -1 for contributions from the purely fermionic sector of the trace of Grassmann-valued matrices. We will solve Eq. (16) in a vertex expansion truncating any generated vertices beyond the Yukawa vertex. The flowing fermion self-energy $\Sigma_f^\Lambda(k_0, \mathbf{k})$ and the boson self-energy $\Sigma_b^\Lambda(q_0, \mathbf{q})$ are parametrized in a derivative expansion keeping the Fermi surfaces fixed.

The cutoff matrix in Eq. (16) is given by

$$R^\Lambda = \text{diag}\left(R_{b,x}^{\Lambda_b}, R_{b,y}^{\Lambda_b}, R_{b,z}^{\Lambda_b}, R_{f1,\uparrow}^{\Lambda_f}, R_{f1,\downarrow}^{\Lambda_f}, -R_{f1,\uparrow}^{\Lambda_f}, -R_{f1,\downarrow}^{\Lambda_f}, \right.$$
$$\left. R_{f2,\uparrow}^{\Lambda_f}, R_{f2,\downarrow}^{\Lambda_f}, -R_{f2,\uparrow}^{\Lambda_f}, -R_{f2,\downarrow}^{\Lambda_f} \right), \quad (18)$$

where one is in principle free to choose the fermion and boson cutoff scales $\Lambda_b(\Lambda)$ and $\Lambda_f(\Lambda)$ and associated regulator functions $R_{b,f}$ independently [26, 27]. The corresponding "flow trajectories" in cutoff space (in the plane of Fig. 7) from the bare action (red dot) to renormalized, effective action (green dot) will be different. We will choose the trajectory along the arrows illustrated in Fig. 7, that is we take $\Lambda_f \to 0$ and $R_f \to 0$ before integrating out order parameter fluctuations which are excluded for momenta smaller than Λ_b. The fermions are however not discarded as in the Hertz theory [5], but coupled self-consistently into the flow for all $\Lambda \in \{\Lambda_b^{\text{UV}}, 0\}$ thereby imposing important boundary conditions for the integration of order parameter fluctuations down the vertical axis in Fig. 7.
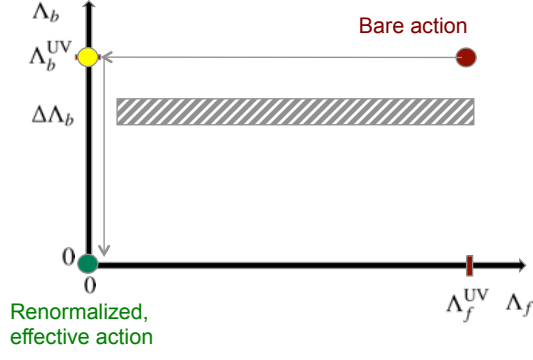
FIG. 7: (Color online) Illustrative flow trajectory in cutoff space. At each step $\Delta\Lambda_b$ of the integration over bosonic momenta along the vertical axis the entire range of fermionic momenta is swept over (grey-striped box).

For the bosons, we use a Litim cutoff for momenta

$$R_{b,x}^{\Lambda_b} = R_{b,y}^{\Lambda_b} = R_{b,z}^{\Lambda_b} = R_b^\Lambda = A_b^\Lambda \left(-\mathbf{q}^2 + \Lambda^2\right)\theta\left(\Lambda^2 - \mathbf{q}^2\right) , \quad (19)$$

where A_b^Λ is bosonic momentum renormalization factor to be specified below. In the following, we will set $\Lambda^b = \Lambda$. The fermionic entries in Eq. (18) are zero.

The fermionic matrix elements of the generalized matrix propagator $\left[\Gamma_R^{(2)\Lambda}[\chi,\bar\chi] + R^\Lambda\right]^{-1}$ occurring in Eq. (16) become:

$$G_{f1,\sigma}^\Lambda(k) = -\langle\psi_{1,\sigma}(k)\bar\psi_{1,\sigma}(k)\rangle^R$$

$$= -\left[\frac{\overrightarrow{\delta}}{\delta\overline\chi(k_1)}\Gamma_R^\Lambda[\chi,\overline\chi]\frac{\overleftarrow{\delta}}{\delta\chi(k_2)} + R^\Lambda\right]^{-1}_{\substack{f1,\sigma \\ \overline\chi=\chi=0 \\ k_1=k_2=k}}$$

$$= \frac{-1}{-ik_0 + \xi_{\mathbf{k},1} + \Sigma_{f1}^\Lambda(k_0,\mathbf{k})} , \quad (20)$$

and analogously for the other flavor and spin components.

The explicitly cutoff-dependent boson propagators are

$$D^R(q) \equiv D_x^R(q) = -\langle\phi_x(q)\phi_x(-q)\rangle^R$$

$$= -\left[\frac{\overrightarrow{\delta}}{\delta\overline\chi(q_1)}\Gamma_R^\Lambda[\chi,\overline\chi]\frac{\overleftarrow{\delta}}{\delta\chi(q_2)} + R^\Lambda\right]^{-1}_{\substack{b,x \\ \overline\chi=\chi=0 \\ q_1=q_2=q}}$$

$$= \frac{-1}{\mathbf{q}^2 + r + \Sigma_b^\Lambda(q_0,\mathbf{q}) + R_b^\Lambda}$$

$$= \begin{cases} \frac{-1}{\mathbf{q}^2+r+\Sigma_b^\Lambda(q_0,\mathbf{q})} & |\mathbf{q}| > \Lambda \\ \frac{-1}{\Lambda^2+r+\Sigma_b^\Lambda(q_0,\mathbf{q})} & |\mathbf{q}| < \Lambda \end{cases} , \quad (21)$$

and analogously for the other spin projections y, z. The functional derivatives are evaluated at zero fields here, as we approach the QCP from the paramagnetic phase.

The flow equation for the fermion self-energy (depicted diagrammatically in Fig. 2) is

$$\partial_\Lambda\Sigma_{f1}^\Lambda[k_0,\mathbf{k}] = 3\left(\lambda^\Lambda\right)^2 \int_{q,R} G_{f2}^\Lambda(k+q)D_b^R(q) , \quad (22)$$

and similarly for flavor 2 upon interchanging $1 \leftrightarrow 2$. We use a short-hand notation encapsulating frequency, momentum integrations and a cutoff derivative with respect to the bosonic cutoff function: $\int_{q,R_b} = \int \frac{dq_0}{2\pi} \int \frac{d^2\mathbf{q}}{(2\pi)^2}\left[-\dot R_b^\Lambda\partial_{R_b^\Lambda}\right]$.

The prefactors and signs of the flow equations are computed by comparing coefficients between the left-hand-side and the right-hand-side of Eq. (16) as outlined in Sec. II of Ref. 28. The 11×11 Grassmann-valued (super-) matrices are evaluated using the GrassmannOps.m package in Mathematica. How to take a supertrace can be found in Ref. 29.

The boson self-energy is determined self-consistently from the particle hole bubble (Fig. 6) at all stages of the flow:

$$\Sigma_b^\Lambda(q_0,\mathbf{q}) = -\left(\Pi^\Lambda(q_0,\mathbf{q}) - \Pi^\Lambda(0,\mathbf{0})\right) \quad (23)$$

$$= 2\left(\lambda^\Lambda\right)^2 \int_k \left[\left(G_{f1}^\Lambda(k+q) - G_{f1}^\Lambda(k)\right)G_{f2}^\Lambda(k)\right.$$

$$\left. + G_{f1}^\Lambda(k)\left(G_{f2}^\Lambda(k+q) - G_{f2}^\Lambda(k)\right)\right]$$

The following ansatz captures the leading frequency and momentum-dependence of the particle-hole bubble:

$$\Sigma_b^\Lambda(q_0,\mathbf{q}) = Z_b^\Lambda|q_0| + A_b^\Lambda\mathbf{q}^2 . \quad (24)$$

At the yellow dot in Fig. 7, the Fermi propagators are still Fermi-liquid like ($\Sigma_{f\alpha}^{\Lambda_{UV}} = 0$) because we have not yet integrated out any order parameter fluctuations which, by Fig. 2, generate a finite fermion self-energy. At that point, the coefficients $Z_b^{\Lambda_{UV}}$, $A_b^{\Lambda_{UV}}$ take finite numerical values. At all stages of the flow, when integrating the flow down the vertical axis of Fig. 7, the bosonic Z-factor and A-factor are determined self-consistently according to the prescription:

$$Z_b^\Lambda = -\left.\frac{\Pi^\Lambda(q_0,\mathbf{0}) - \Pi^\Lambda(q_0,\mathbf{0})}{q_0}\right|_{q_0=\Lambda}$$

$$A_b^\Lambda = 1 - \left.\frac{\Pi^\Lambda(0,\mathbf{q}) - \Pi^\Lambda(0,\mathbf{0})}{\mathbf{q}^2}\right|_{q_x=\Lambda,q_y=0} . \quad (25)$$

This allows them to pick up potentially singular renormalizations during the flow. The boson momentum factor is isotropic in momentum space; interchanging $q_x \leftrightarrow q_y$ delivers the same value for A_b^Λ.

The flow equation as per Fig. 2 for the Yukawa coupling is

$$\partial_\Lambda\lambda^\Lambda = -\left(\lambda^\Lambda\right)^3 \int_{q,R} G_{f1}^\Lambda(k+q)G_{f2}^\Lambda(k+q)D_b^R(q)\Big|_{k_0=0,\mathbf{k}=\mathbf{k}_{HS}} . \quad (26)$$

We now give the explicit expressions of the flow equations (22,23,26). To that end, it is convenient to use the rescaled variables $\tilde Z_b^\Lambda = \frac{Z_b^\Lambda}{\Lambda}$, $\tilde\xi_{\mathbf{k},1} = \frac{\xi_{\mathbf{k},1}}{\Lambda}$ as well as rescaled momenta: $\tilde k_0 = \frac{k_0}{\Lambda}$, $\tilde q_0 = \frac{q_0}{\Lambda}$, $\tilde q_x = \frac{q_x}{\Lambda}$, and $\tilde q_y = \frac{q_y}{\Lambda}$.

For the the fermionic frequency exponent, there is

$$\eta_{Z_{f1}} = 3\left(\tilde{\lambda}^\Lambda\right)^2 \sqrt{|v_{f1}^\Lambda||v_{f2}^\Lambda|} \int_{-1}^{1} \frac{d\tilde{q}_y}{2\pi} \int_{-\sqrt{1-\tilde{q}_y^2}}^{+\sqrt{1-\tilde{q}_y^2}} \frac{d\tilde{q}_x}{2\pi} \int_{-\infty}^{\infty} \frac{d\tilde{q}_0}{2\pi} 2A_b^\Lambda \frac{1}{\left(i\tilde{q}_0 - |v_{f2}^\Lambda|\tilde{\xi}_{\mathbf{k}_{HS}+\tilde{\mathbf{q}},2}\right)^2} \frac{1}{\left(\tilde{Z}_b^\Lambda|\tilde{q}_0| + A_b^\Lambda\right)^2} \,, \tag{27}$$

and similarly $(1 \leftrightarrow 2)$ for flavor 2. The frequency integral over $\tilde{q}_0$ can be performed analytically so that at each step of the flow, two-dimensional integrations over $\tilde{q}_x$ and $\tilde{q}_y$ have to be performed numerically. The Yukawa anomalous exponent contains fermion propagators of both flavors:

$$\eta_{\text{yuk}} = -\left(\tilde{\lambda}^\Lambda\right)^2 \sqrt{|v_{f1}^\Lambda||v_{f2}^\Lambda|} \int_{-1}^{1} \frac{d\tilde{q}_y}{2\pi} \int_{-\sqrt{1-\tilde{q}_y^2}}^{+\sqrt{1-\tilde{q}_y^2}} \frac{d\tilde{q}_x}{2\pi} \int_{-\infty}^{\infty} \frac{d\tilde{q}_0}{2\pi} 2A_b^\Lambda \frac{1}{i\tilde{q}_0 - |v_{f1}^\Lambda|\tilde{\xi}_{\mathbf{k}_{HS}+\tilde{\mathbf{q}},1}} \frac{1}{i\tilde{q}_0 - |v_{f2}^\Lambda|\tilde{\xi}_{\mathbf{k}_{HS}+\tilde{\mathbf{q}},2}} \frac{1}{\left(\tilde{Z}_b^\Lambda|\tilde{q}_0| + A_b^\Lambda\right)^2} \,. \tag{28}$$

For the flow of the fermionic momentum factors we use the projected k_x and k_y derivatives of Eq. (22)

$$\partial_\Lambda A_{f1,x}^\Lambda = n_{k_x,1}\partial_{k_x}\partial_\Lambda\Sigma_{f1}^\Lambda[k_0,\mathbf{k}]\Big|_{k_0=0,\mathbf{k}=\mathbf{k}_{HS}}$$
$$\partial_\Lambda A_{f1,y}^\Lambda = n_{k_y,1}\partial_{k_y}\partial_\Lambda\Sigma_{f1}^\Lambda[k_0,\mathbf{k}]\Big|_{k_0=0,\mathbf{k}=\mathbf{k}_{HS}} \tag{29}$$

with the initial conditions $A_{f1,x}^{\Lambda_{UV}} = A_{f1,y}^{\Lambda_{UV}} = 1$. The Fermi surface normal projector is (similarly for flavor 2)

$$n_{k_{x/y},1} = \frac{2t_{1,x/y}\sin k_{x/y}}{\sqrt{\left(2t_{1,x}\sin k_{x/y}\right)^2 + \left(2t_{1,y}\sin k_y\right)^2}} \,. \tag{30}$$

The flow equations for the rescaled variables are $\tilde{A}_{f1,x}^\Lambda = \frac{A_{f1,x}^\Lambda}{Z_{f1}^\Lambda}$,

$\tilde{A}_{f1,y}^\Lambda = \frac{A_{f1,y}^\Lambda}{Z_{f1}^\Lambda}$. With $\eta_{Z_{f1}}$ given in Eq. (27), these take the form

$$\Lambda\partial_\Lambda\tilde{A}_{f1,x}^\Lambda = \left(\eta_{Z_{f1}} - \eta_{A_{f1,x}}\right)\tilde{A}_{f1,x}^\Lambda$$
$$\Lambda\partial_\Lambda\tilde{A}_{f1,y}^\Lambda = \left(\eta_{Z_{f1}} - \eta_{A_{f1,y}}\right)\tilde{A}_{f1,y}^\Lambda \,, \tag{31}$$

with the exponents $\eta_{A_{f1,x}} = -\frac{d\log A_{f1,x}^\Lambda}{d\log\Lambda}$, $\eta_{A_{f1,y}} = -\frac{d\log A_{f1,y}^\Lambda}{d\log\Lambda}$. At every step of the flow, we compute then per Eq. (6)

$$|v_{f1}^\Lambda| = \frac{\sqrt{\left(\tilde{A}_{f1,x}^\Lambda\right)^2 + \left(\tilde{A}_{f1,y}^\Lambda\right)^2}}{|\nabla\xi_{1,\mathbf{k}}|_{\mathbf{k}=\mathbf{k}_{HS}}} \,. \tag{32}$$

Expressions for the exponents:

$$\eta_{A_{f1,x}} = -n_{k_{HS,x},1} 3\left(\tilde{\lambda}^\Lambda\right)^2 \sqrt{|v_{f1}^\Lambda||v_{f2}^\Lambda|} \frac{|v_{f2}^\Lambda|}{\tilde{A}_{f1,x}} \int_{-1}^{1} \frac{d\tilde{q}_y}{2\pi} \int_{-\sqrt{1-\tilde{q}_y^2}}^{+\sqrt{1-\tilde{q}_y^2}} \frac{d\tilde{q}_x}{2\pi} \int_{-\infty}^{\infty} \frac{d\tilde{q}_0}{2\pi} 2A_b^\Lambda \frac{2t_{2x}\sin(k_{HS,x}+\tilde{q}_x\Lambda)}{\left(i\tilde{q}_0 - |v_{f2}^\Lambda|\tilde{\xi}_{\mathbf{k}_{HS}+\tilde{\mathbf{q}},2}\right)^2} \frac{1}{\left(\tilde{Z}_b^\Lambda|\tilde{q}_0| + A_b^\Lambda\right)^2}$$

$$\eta_{A_{f1,y}} = -n_{k_{HS,y},1} 3\left(\tilde{\lambda}^\Lambda\right)^2 \sqrt{|v_{f1}^\Lambda||v_{f2}^\Lambda|} \frac{|v_{f1}^\Lambda|}{\tilde{A}_{f1,y}} \int_{-1}^{1} \frac{d\tilde{q}_y}{2\pi} \int_{-\sqrt{1-\tilde{q}_y^2}}^{+\sqrt{1-\tilde{q}_y^2}} \frac{d\tilde{q}_x}{2\pi} \int_{-\infty}^{\infty} \frac{d\tilde{q}_0}{2\pi} 2A_b^\Lambda \frac{2t_{2y}\sin(k_{HS,y}+\tilde{q}_y\Lambda)}{\left(i\tilde{q}_0 - |v_{f2}^\Lambda|\tilde{\xi}_{\mathbf{k}_{HS}+\tilde{\mathbf{q}},2}\right)^2} \frac{1}{\left(\tilde{Z}_b^\Lambda|\tilde{q}_0| + A_b^\Lambda\right)^2} \,. \tag{33}$$

Finally, the (rescaled) boson frequency factor and momentum factor are self-consistently determined from

$$\tilde{Z}_b^\Lambda = 2\left(\tilde{\lambda}^\Lambda\right)^2 \sqrt{|v_{f1}^\Lambda||v_{f2}^\Lambda|} \int_{-\pi}^{\pi} \frac{dk_x}{2\pi} \int_{-\pi}^{\pi} \frac{dk_y}{2\pi} \frac{1}{\Lambda^2} \int_{-\infty}^{\infty} \frac{d\tilde{k}_0}{2\pi} \left[\left(\frac{1}{i(\tilde{k}_0+1) - |v_{f1}^\Lambda|\xi_{\mathbf{k},1}} - \frac{1}{i\tilde{k}_0 - |v_{f1}^\Lambda|\xi_{\mathbf{k},1}}\right)\frac{1}{i\tilde{k}_0 - |v_{f2}^\Lambda|\xi_{\mathbf{k},2}} + (1 \leftrightarrow 2)\right]$$

$$\tilde{A}_b^\Lambda = 2\left(\tilde{\lambda}^\Lambda\right)^2 \sqrt{|v_{f1}^\Lambda||v_{f2}^\Lambda|} \int_{-\pi}^{\pi} \frac{dk_x}{2\pi} \int_{-\pi}^{\pi} \frac{dk_y}{2\pi} \frac{1}{\Lambda^2} \int_{-\infty}^{\infty} \frac{d\tilde{k}_0}{2\pi} \left[\left(\frac{1}{i\tilde{k}_0 - |v_{f1}^\Lambda|\xi_{\mathbf{k}+q_x,1}} - \frac{1}{i\tilde{k}_0 - |v_{f1}^\Lambda|\xi_{\mathbf{k},1}}\right)\frac{1}{i\tilde{k}_0 - |v_{f2}^\Lambda|\xi_{\mathbf{k},2}} + (1 \leftrightarrow 2)\right]_{q_x=\Lambda} \,. \tag{34}$$

Eqs. (3,27,28,31,33,32,34) are solved numerically as a function of flow parameter $\Lambda = \Lambda^{UV}e^{-s}$ so that $s = 0$ corresponds to the UV ($\Lambda^{UV} = 1$). The hotspot coordinates are $k_{HS,x} = 1.0472$, $k_{HS,y} = 2.0944$. As initial conditions, we choose $\lambda^{\Lambda_{UV}} = 0.25$, $Z_{f1}^{\Lambda_{UV}} = Z_{f2}^{\Lambda_{UV}} = 1$, and $A_{f1}^{\Lambda_{UV}} = A_{f2}^{\Lambda_{UV}} = 1$. The initial values for the boson propagator are $\tilde{Z}_b^{\Lambda_{UV}} = 0.052$ and $\tilde{A}_b^{\Lambda_{UV}} = 1.011$.